Measuring Soft Tissue Elasticity by Monitoring Surface Acoustic Waves Using Image Plane Digital Holography

Shiguang Li[1] and Amy L. Oldenburg[1,2,]*

[1]*Department of Physics and Astronomy,* [2]*Biomedical Research Imaging Center,*
University of North Carolina at Chapel Hill, Chapel Hill, NC 27599

ABSTRACT

The detection of tumors in soft tissues, such as breast cancer, is important to achieve at the earliest stages of the disease to improve patient outcome. Tumors often exhibit a greater elastic modulus compared to normal tissues. In this paper, we report our first study to measure elastic properties of soft tissues by mapping the surface acoustic waves (SAWs) with image plane digital holography. The experimental results show that the SAW velocity is proportional to the square root of elastic modulus over a range from 3.7-122kPa in homogeneous tissue phantoms, consistent with Rayleigh wave theory. This technique also permits detection of the interface of two-layer phantoms 10mm deep under surface and the interface depth by quantifying the SAW dispersion.

Keywords: Holography, Surface acoustic wave (SAW), Rayleigh wave, Dispersion, Elasticity, Young's modulus, Tumor, Tissue

1. INTRODUCTION

The detection of cancer at the earliest stage is critical to improve patient outcome. Currently, cancer is detected by Computed Tomography (CT) or Magnetic Resonance Imaging (MRI) [1]. These imaging technologies have limited application for routine screening applications because of their high cost, and, in the case of CT, the associated radiation dose. In breast cancer in particular, malignant tissues exhibit a greater elastic modulus (Young's modulus) compared to normal tissues [2]. This property has been the source of great interest in the development of novel elastography techniques, *i.e.*, techniques that image tissue elastic properties. Ultrasound is a popular tool to obtain the elasticity distribution inside the human body, but its measurement resolution is only in the millimeter range [3], which may miss micrometer-sized calcifications. Optical coherence elastography [4] is an emerging technology with micrometer resolution, but with penetration depth limited to 1~2mm for highly scattering tissues [5]. The diffuse optical tomography is another emerging technology to measure the elastic tissues; however it suffers from poor spatial resolution [6].

Here we investigate a new elastography method based on monitoring surface acoustic waves (SAWs) arising from an applied force, the propagation of which are closely related to the material's elasticity. This phenomenon has found wide applications in seismology to detect earthquakes [7] and in non-destructive testing to detect the defects inside materials or multi-layer samples [8]. In biomedicine, some researchers have studied the SAW velocity with laser Doppler vibrometry [9, 10], and the tissues' inhomogeneity with optical holographic technology [11-13]. Unfortunately this research either only provided single point detection or did not reveal the relationship between the tissues' inhomogeneity and the SAW properties. In cancer diagnosis, it is of great interest to translate holographic technology toward a novel elastography tool as it has the potential to provide high measurement resolution, fast speed, low cost, and a large area of assessment. Another advantage of the combination of SAWs and holographic technology is its potential to non-invasively detect tumors deep under surface, as the SAWs extend into the material approximately one SAW wavelength deep [7, 8]. To apply this optical technology as a practical diagnosis tool, we must fully understand the relationship between the SAWs as measured by holographic technology and the elastic properties of tissues. These relationships will become the basis to detect tumors under the tissue surface using this novel optical elastography technique. In this paper we introduce our first study about their relationships. A digital holographic system is applied where a high-speed digital camera, rather than the traditional photosensitive plate, is used as a recording medium.

2. SAMPLE PREPARATION

Tissue phantoms with optical scattering coefficients and elasticity similar to real tissues are used in our experiments [14]. The phantoms were fabricated from a mixture of pure polydimethylsiloxane (PDMS) fluid (50 cSt viscosity, ClearCo, Inc.), and a room- temperature vulcanizing silicone and its associated curing agent (General Electric RTV-615 A and B, respectively, Circuit Specialists, Inc.). The elastic moduli of the phantoms were adjusted by changing the ratio of pure PDMS and vulcanizing silicone over the range from 15:1-1:1. The ratio between the vulcanizing silicone and its curing agent was constant at 10:1. Titanium dioxide (TiO_2) powder (Sigma-Aldrich, #224227, mean size 1 μm, <5 μm) were embedded with a concentration of 4mg/g in the tissue phantoms to function as optical scatterers for holographic imaging. The phantom solutions were mixed thoroughly on an ultrasonicator for several tens of minutes at room temperature and then poured into a 5" diameter plastic container, with a thickness of approximately 30 mm. The phantoms dimensions were chosen to be large to eliminate significant boundary reflections. All phantoms were cured at 80°C for one day and subsequently at room temperature for another day.
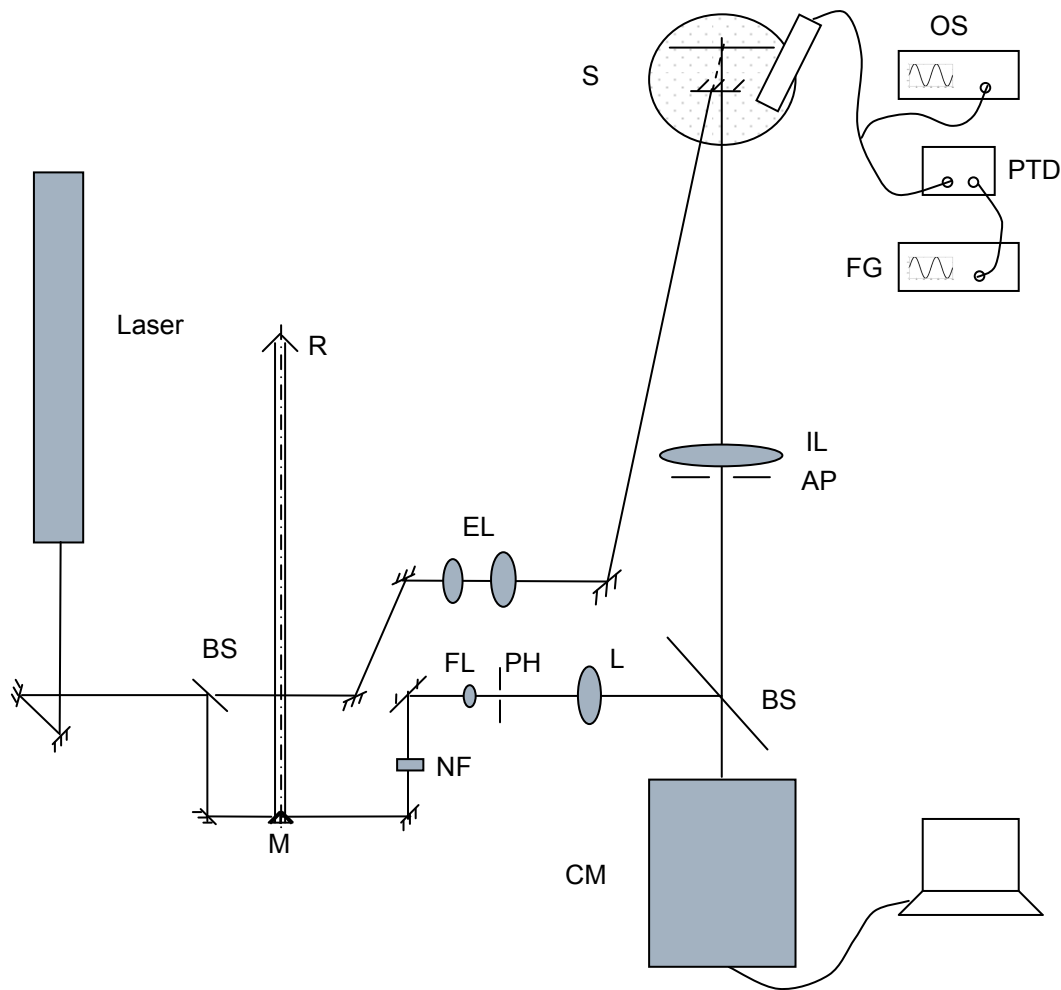
3. EXPERIMENTAL SETUP

Fig.1 Schematic diagram of holographic experimental setup. BS: beam splitter, M: two small mirror prisms, R: retroreflector, NF: neutral filter, FL: focusing lens, PH: pinhole, L: lens, EL: expanding lens, IL: imaging lens, AP: aperture, CM: fast speed camera, S: sample, OS: Oscilloscope, PTD: piezo transducer driver, FG: function generator.

Figure 1 shows the experimental setup to measure the SAWs. This is an image plane holographic system. A HeNe beam with 5mW (Thorlabs) power is split by a 92:8 beamsplitter. The majority of the optical power goes along the measurement arm to the phantom through two optical lenses. By adjusting the distance from lens to lens and from lens to phantom, the illumination area can be adjusted. In our experiments, the output from the last lens is chosen to be slightly divergent. The diffusely scattered light from the phantom is imaged onto the sensor of a fast CMOS camera (Photron SA3) with an imaging lens. In experiments, the camera frame rate is adjusted as 1, 2, 3, and 7.5 KHz. The corresponding pixel array is 1024×1024, 640×640, 512×512, and 256×256. The pixel size is 17μm, and the imaging area for the full 1024×1024 pixel array is 16×16mm^2. As there are highly modulated speckles in the image, an adjustable aperture is placed close to the imaging lens. When the Airy disc resulting from the aperture covers several pixels, the impact of speckles is almost completely filtered out. The reference arm with lower power passes through a spatial filter, *i.e.*, the combination of a short focal length lens and a pinhole, and a positive lens, before being directed into the camera. The distance from the pinhole to the lens is adjusted so that the interference fringes between reference and sample could be identified over the whole measurement area. As the optical path of an edge ray from the sample is greater than that of a central ray, the output light from the lens L is chosen to be divergent. Ideally, the optical path difference (OPD) between the edge ray and the central ray should be balanced for the two arms.

The image of the phantom interacts with the reference beam, forming a local holographic image. The image is recorded on the computer for further investigation. A neutral density filter is inserted in the reference arm to adjust the pattern contrast. A retro-reflector is used to adjust the optical path so that the OPD between the two arms is within the coherence length of the laser, ~200mm. A piezo-electric transducer with a travel range of 40μm is placed in contact with the sample, and driven by a high voltage supply that is controlled by a function generator, which drives the piezo sinusoidally at frequencies ranging from 40-900Hz. Figure 2(a) shows an example interference pattern. It should be noted that there are background fringes (from lower left to upper right) evenly distributed in the image that are caused by the protection glass in front of the camera. These are stationary, and do not affect the measurement result if we apply a phase shifting algorithm, as described below.
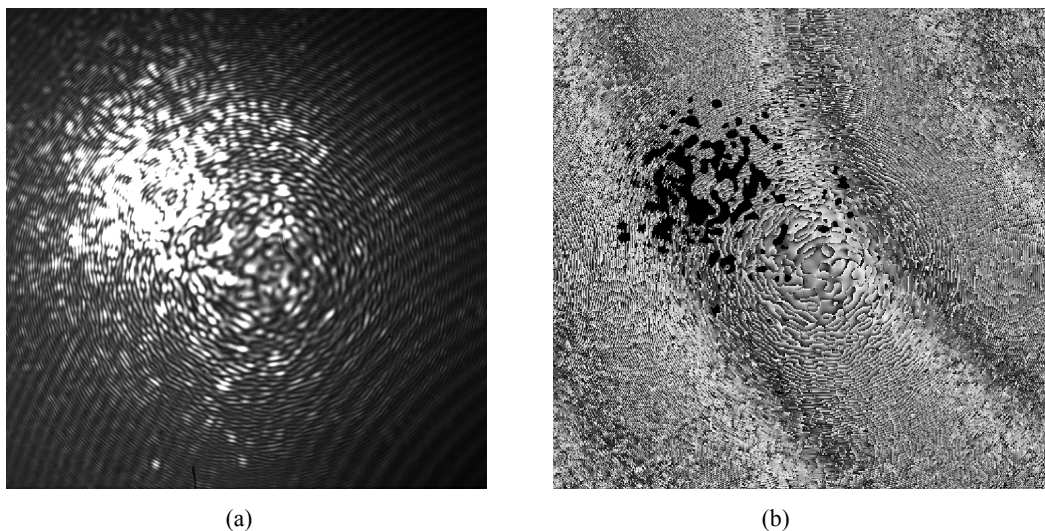

(a)	(b)

Fig. 2 Images of a phantom during mechanical excitation by a piezo-electric transducer with a driving frequency of 300Hz. The camera frame rate is 3KHz and the measurement area is 8mm. (a) One frame of the holographic image recorded by the camera, (b) the extracted SAW image according to the algorithm described below.

4. RESULTS

4.1 SAW extraction algorithm

The point-like force caused by the piezo acts on the phantoms, generating SAWs that propagate radially outward from the point of actuation. When the phantom's thickness is much greater than the SAW wavelength, the SAW is well-described as a Rayleigh wave [15]. In two dimensions, the displacement in the z direction (out of plane) can be expressed as $h = A\cos(\omega t + kx)$, where A is the amplitude, x is one of the transverse dimensions, ω is the temporal frequency (given by the piezo frequency during harmonic excitation, or by the apparent SAW frequency during impulse excitation) and k is the spatial frequency.

For our image plane holographic system, the interference fringes are localized, *i.e.*, the displacement at a certain position x will only affect the phase at the corresponding position in the image plane. Generally, the intensity of the interference pattern with reflective illumination is:

$$I = I_{dc} + I_{ac}\cos(\phi_{SAW}(x,t) + \Delta\phi(x)) \tag{1}$$

where $\phi_{SAW}(x,t) = \dfrac{4\pi}{\lambda_{la}}A\cos(\omega t + kx)$, I_{dc} is the mean intensity in the image, I_{ac} is the amplitude of intensity variation, λ_{la} is the laser wavelength, and $\Delta\phi$ is the phase difference between the sample and reference when it is stationary (in the absence of SAWs). The spatial variation of $\Delta\phi$ (that gives rise to speckles) is minimized by using the aperture after the imaging lens.

There are two main algorithms to extract the phase for image plane holography: Fourier transform and phase shifting algorithm [16, 17]. We applied the phase shifting algorithm in these experiments. Traditionally, the phase shifting is realized by changing the delay of the reference arm with a piezo. However, we realized that the time-periodic modulation provided by SAWs can be used directly as the phase shift. For simplicity, here we used three successive frames acquired with at equal time intervals to extract the phase. The phase is expressed as [16]:

$$\phi_{SAW} = \arctan\left(\frac{I_1 - I_3}{I_1 + I_3 - 2I_2}\tan\left(\frac{\alpha}{2}\right)\right) \tag{2}$$

where I_i (i=1~3) is the optical intensity in three frames, and α is the temporal phase difference (ωt) between two adjacent frames. The measurement results show that this method can effectively identify the positions of the SAW peaks and valleys. It should be noted that, as there is a peak and a valley in one SAW period, the apparent wavelength directly from application of Eq. (2) is half of the real value. Figure 2(b) shows the phase image of (a).

4.2 Mechanical response of phantoms with varying Young's modulus

When a semi-infinite homogeneous material is excited by a mechanical impulse, SAWs will propagate from the point of actuation. The velocity of the SAW depends on the Young's modulus and density of the material according to [9]:

$$v = \frac{1}{1.05}\sqrt{\frac{E}{3\rho}} \tag{3}$$

We performed measurements of homogeneous phantoms by tracking the apparent SAW velocity on the phase image after excitation by a mechanical impulse. Measurements were performed in homogeneous phantoms with Young's modulus ranging from 3.7-122kPa to match the range of elastic moduli encountered in most soft tissue such as the human breast [18]. We found the SAW velocity was dependent on the square root of the Young's modulus as predicted by equation (3), as shown in Figure 3. The measured slope was 0.017, which is within 2% of the theoretical slope of 0.0174 according to equation (3), assuming the phantom's density is 1000kg/m^3.
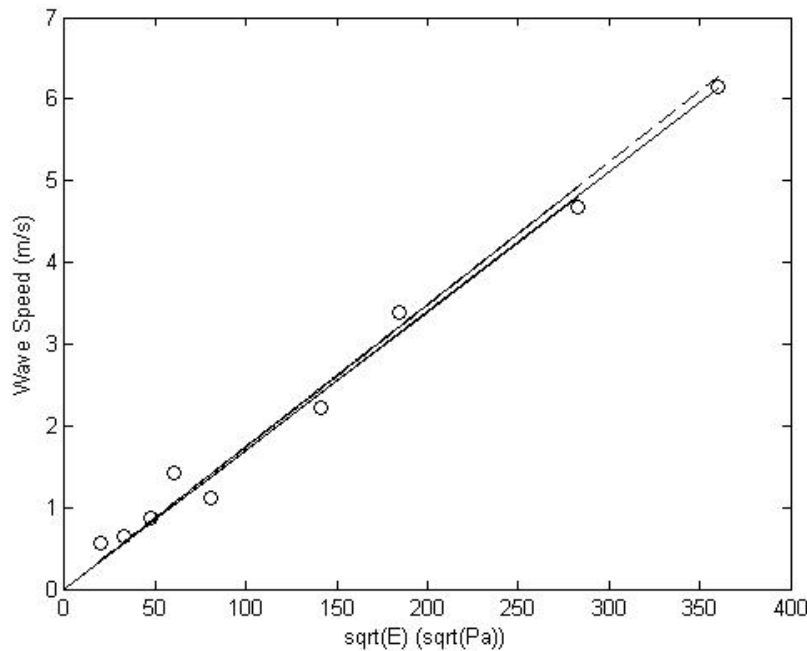
Fig. 3 The variation in SAW speed as a function of the square root of the Young's modulus in homogeneous tissue phantoms. Solid curve: best-fit line, dashed curve: relationship according to equation (3).

4.3 SAW propagation in two-layer phantoms

When there is inhomogeneity in phantoms, there will be dispersion in the SAW velocity [8]. In order to investigate the potential to measure depth-dependent elasticity from SAW velocity dispersion, we analyzed two-layer phantoms (Figure 4). The Young's modulus E of the upper layer was 38kPa, and the lower layer was 10.5kPa. The SAW velocity, if in a homogeneous material of elasticity equal to each of the layers, would be 1.8m/s at 10.5kPa and 3.4m/s at 38kPa according to Eq.(3). The thickness of the lower layer was about 30mm for the two phantoms, and the upper layer for the first phantom was ~10mm thick, and the second was ~5mm thick. The measured SAW speed and the corresponding wavelength at different driving frequencies are plotted in Figure 4. From the velocity plots, it can be seen that the velocity varies from close to the predicted velocity of the lower layer (~1.5m/s) to close to the predicted velocity of the upper layer (~3.5m/s), when the frequency increases. This behavior is expected because at high frequencies the SAW wavelength is short and does not penetrate into the lower layer. At low frequencies the SAW wavelength is large and, at the extreme, is dominated with the thick lower layer. The transition between these two extremes is expected to occur when the SAW wavelength is approximately equal to the upper layer thickness (see dashed lines on Figure 4); for the first phantom with ~10mm thick layer, it should occur at a low frequency (~200Hz) in comparison to the ~5mm thick layer in the second phantom, where the transition occurs at a higher frequency (~400Hz). We note some variation in velocity that will be a topic of future investigation. In general, this experiment proves that the SAW dispersion is useful for detecting variation in tissue elasticity at depths up to 10mm.
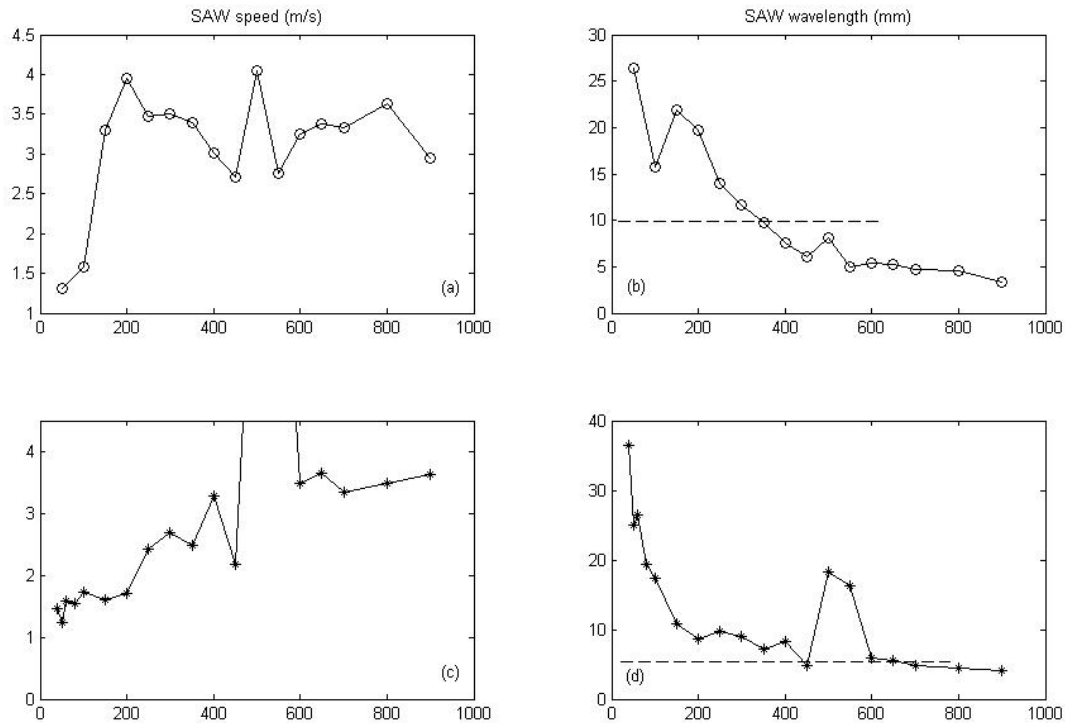
Fig. 4 SAW speed and wavelength varies with the piezo driving frequency. (a) & (b) are the data for a two-layer phantom with 10mm thick upper layer, (c) &(d) are for a two-layer phantom with 5mm thick upper layer.. The *x* axis for 4 plots is piezo driving frequency, and the *y* axis for both columns is shown on the top. The Young's modulus *E* for the upper layer is 38kPa, corresponding to SAW speed 3.4m/s, and that for the lower layer is 10.5kPa, corresponding to SAW speed 1.8m/s.

5. CONCLUSIONS

Studying the mechanical properties of soft tissues may aid in the detection of abnormal tissues. The elasticity of tissue phantoms was experimentally studied by measuring the SAW velocity with a high speed digital holographic system. The experimental results show that the velocity of SAWs is proportional to the square root of Young's modulus in the range of 3.7-122kPa. The ratio between the square root of the Young's modulus and the SAW velocity is within 2% of the theoretical value. Two-layer phantoms were investigated by measuring the SAW velocity dispersion. The experiments successfully identified the interface between the layers located ~10mm deep. These results indicate that this holographic technology is very promising as a novel elasticity diagnosis tool. The future work is 1) to enlarge the measurement area in order to track one SAW at a relatively long time, which may provide richer information than the local SAW, 2) to study the relationship between the SAW and the local elasticity perturbation, and 3) to characterize the measurement resolution and accuracy when quantifying a tumor-like inhomogeneity under the tissue surface.

REFERENCES

[1] http://www.ucsfhealth.org/adult/medical_services/cancer/brain/conditions/brain_tumor/diagnosis.html
[2] Samani, A., Zubovits, J. and Plewes D, "Elastic moduli of normal and pathlogical human breast tissues: an inversion-technique-based investigation of 169 samples," Phys. Med. Biol. 52, 1565-1576 (2007).

[3] Rownd, J. J., Madsen, E. L., Zagzebski, J. A., Frank, G. R. and Dong, F., "Phantoms and automated system for testing the resolution of ultrasound scanners," Ultrasound in Med. & Biol. 23(2), 245-260 (1997).

[4] Kirkpatrick, S. J., Wang R. K. and Duncan D. D., "OCT-based elastography for large and small deformations," Opt. Express 14(24), 11585-11597 (2006).

[5] Schmitt, J. M., "Optical coherence tomography (OCT): A review," IEEE J Sel. Top. Quant. 5(4), 1205-1215 (1999).

[6] Gibson, A. P., Hebden, J. C. and Arridge, S. R., "Recent advances in diffuse optical imaging," Phys. Med. Biol. 50, R1-R43 (2005).

[7] Harkrider, D. G., "Surface waves in multilayered elastic media I. Rayleigh and Love waves from buried sources in a multilayered elastic half-space," B. Seismol. Soc. Am 52(2), 627-679 (1964).

[8] Szabo, T. L., "Obtaining subsurface profiles from surface-acoustic-wave velocity dispersion," J. Appl. Phys. 46(4), 1448-1454 (1975).

[9] Zhang, X. and Greenleaf, J. F., "Estimation of tissue's elasticity with surface wave speed (L)," J. Acoust. Soc. Am. 122(5), 2522-2525 (2007).

[10] Royston T. J., Mansy, H. A. and Sandler R. H., "Excitation and propagation of surface waves on a viscoelastic half-space with application to medical diagnosis," J. Acoust. Soc. Am. 106(6), 3678-3686 (1999).

[11] Schedin S., Pedrini, G. and Tiziani H. J., "Pulsed digital holography for deformation measurements on biological tissues," Appl. Optics 39(16), 2853-2857 (2000).

[12] Woisetschlager, J., Sheffer, D. B., Loughry C. W., Somasundaram, K., Chawla, S. K. and Wesolowski, P. J., "Phase-shifting holographic interferometry for breast cancer detection," Appl. Opt. 33 (22), 5011-5015 (1994).

[13] Hernández-Montes, M. del S., Pérez-López, C. and Santoyo, F. M., "Finding the position of tumor inhomogeneities in a gel-like model of a human breast using 3-D pulsed digital holography," J. Biomed. Opt 12(2), 024027 (2007).

[14] Liang, X., Oldenburg, A. L., Crecea, V., Chaney, E. J. and Boppart, S. A., "Optical micro-scale mapping of dynamic biomechanical tissue properties," Opt. Express 16(15), 11052-11065 (2008).

[15] Auld, B. A., [Acoustic Fields and Waves in Solids] II, Krieger Publishing Company, Malabar, Florida, 85-100 (1990).

[16] Pedrini, G., Tiziani, H. J. and Zou, Y., "Digital double pulse-TV-holography," Opt. Laws in Eng. 26, 199-219 (1997).

[17] Hipp, M., Woisetschläger, J., Reiterer, P. and Neger T., "Digital evaluation of interferograms," Measurement 36, 53-66 (2004).

[18] Crecea, V., Oldenburg, A. L., Liang, X., Ralston, T. S. and Boppart, S. A., "Magnetomotive nanoparticle transducers for optical rheology of viscoelastic materials," Opt. Express 17(25): 23114-23122 (2009).